

Theoretical model for magnetooptic imaging

L.E. Helseth

Department of Physics, University of Oslo, P.O. Box 1048 Blindern, N-0316 Oslo, Norway

email: l.e.helseth@fys.uio.no

PACS: 75.70.-i, 78.20.Ls

Keywords: Magneto-optical effects, Thin films, Type-II superconductivity

Abstract

A theoretical model for magnetooptic imaging is presented. The model gives a detailed description of the magnetooptic indicator and the optical imaging system, where the intensity at the detector plane is described by a set of diffraction integrals. To demonstrate the applicability of the model, some issues concerning imaging of single vortices in superconductors are studied. It is found that the useful signal is strongly dependent on the penetration depth of the superconductor, and also the sensitivity and thickness of the indicator.

I. INTRODUCTION

For centuries humans have tried to 'see' magnetic fields using various devices. Iron particles, magnetic fluids, inductive coils, Hall probes and magnetic bacterias are only a few of the approaches which have been adopted. During the past 40 years the research on magneto-optic visualization has been highly motivated by the need to 'see' magnetic fields from superconductors. To that end, magneto-optic visualization using thin film indicators has been particularly useful. In 1957 P.B. Alers visualized for the first time the magnetic field distribution in a superconductor using a mixture of cerous nitrate-glycerol [1]. A highly successful development followed in 1968 when H. Kirchner noticed that chalcogenide-films could be used to visualize fields with improved sensitivity [2]. In the following 20 years magneto-optic studies were published periodically, mainly looking at flux profiles in superconductors [3,4]. However, there were no major advances until 1991, when it was discovered that bismuth-substituted iron garnet films with in-plane magnetization are excellent indicators with almost no domain activity [5–7]. This discovery triggered a large number of quantitative investigations of the flux behaviour in high-temperature superconductors [8–10]. Two of the most recent advances in this field are ultrafast magneto-optical studies (see e.g. ref. [11]) and imaging of single vortices [12].

Although magneto-optical indicators have mainly been used to image magnetic fields from superconductors, a large number of other possible application areas exists. Thus, it has been realised that such indicators are useful for imaging magnetic defects, magnetic phase transitions, microelectronic circuits and magnetic storage media [13–18].

Since the field of magneto-optic visualization has matured for more than 40 years, one may expect that most parts of the image formation process is well understood. This is not the case. In fact, only recently a model for magneto-optic imaging has been published [18]. However, this model is mostly concerned with the magnetization redistribution in the indicator. The purpose of the current paper is to develop a more detailed model for the magneto-optic imaging system (see Fig. 1), including the indicator, and to use this to examine the possibility of imaging weak magnetic fields, e.g. single vortices in superconductors.

II. MAGNETIZATION IN THE INDICATOR

The basic sensor element for detection of magnetic fields is the magneto-optic indicator. It is therefore first necessary to know how the indicator respond to an external field [18]. Let \mathbf{M} be the magnetization vector in the indicator, and M_s be the saturation magnetization. Then we have from Fig. 2

$$\mathbf{M} = M_s[\cos\beta\cos\phi_M, \cos\beta\sin\phi_M, \sin\beta] = [M_r\cos\phi_M, M_r\sin\phi_M, M_z] \quad . \quad (1)$$

The external field is given by

$$\mathbf{H} = [H_r\cos\phi_H, H_r\sin\phi_H, H_z] \quad , \quad (2)$$

where $M_r = \sqrt{M_x^2 + M_y^2}$ and $H_r = \sqrt{H_x^2 + H_y^2}$. We assume that the indicator consists of a single domain, and that its free energy can be expressed as a sum of the uniaxial anisotropy energy (E_u), the Zeeman energy (E_z) and the demagnetizing energy (E_d)

$$E = E_u + E_z + E_d . \quad (3)$$

The uniaxial anisotropy energy can be written as,

$$E_u = K_u \cos^2 \beta , \quad (4)$$

where K_u is the uniaxial anisotropy constant. The Zeeman energy is given as

$$E_z = -\mu_0 \mathbf{M} \cdot \mathbf{H} = -\mu_0 M_s [H_r \cos \beta \cos(\phi_M - \phi_H) + H_z \sin \beta] . \quad (5)$$

Since we neglect the cubic anisotropy of the indicator the in-plane magnetization direction must be the same as that of the external field ($\phi_M = \phi_H$). The demagnetizing energy, which tends to keep the magnetization in the plane of the film, can be given as

$$E_d = \frac{\mu_0 M_s^2}{2} \sin^2 \beta . \quad (6)$$

Minimizing E with respect to β results in the following relationship

$$H_a \sin \beta \cos \beta + H_r \sin \beta - H_z \cos \beta = 0 , \quad (7)$$

where the so-called anisotropy field is given by

$$H_a = M_s - \frac{2K_u^{tot}}{\mu_0 M_s} . \quad (8)$$

If we assume that $H_r = 0$, then the resulting expression for the magnetization is

$$M_r = M_s \sqrt{1 - \left(\frac{H_z}{H_a}\right)^2} , H_z \leq H_a , \quad (9)$$

and

$$M_z = M_s \frac{H_z}{H_a} , H_z \leq H_a . \quad (10)$$

If β is very small (corresponding to very small H_z , or large H_a or H_r), we may put $\sin \beta \approx \beta$ and $\cos \beta \approx 1$, and the magnetization becomes

$$M_r \approx M_s , H_z \ll H_a , \quad (11)$$

and

$$M_z \approx M_s \frac{H_z}{H_a + H_r} , H_z \ll H_a , \quad (12)$$

Thus we see that an in-plane component H_r will only reduce the z-component of the magnetization. Therefore, it is necessary to keep H_r and H_a small if large sensitivity to H_z is needed.

III. THE MAGNETOOPTIC IMAGING SYSTEM

The basic imaging system is shown in Fig.1. In principle, it is a conventional polarizing microscope, although many different designs exists [12]. Basically, the z-component (or any other component) of the magnetization is converted into a small rotation of the plane of polarization, which can then be detected by an array detector (e.g. CCD). The signal on the detector can be found by an analysis based on Jones matrices together with the methods used in refs. [19,20]. For a general polarization distribution incident on the objective we write [20]

$$\mathbf{E}_0 = \begin{bmatrix} a(\theta, \phi) \\ b(\theta, \phi) \end{bmatrix} ,$$

where θ is the incident angle and ϕ is the azimuthal angle. In this paper we assume that the incident polarization after the polarizer consists of a x-component only ($a=1$ and $b=0$). The effect of the objective lens is to change the incident polarization into s and p-polarized light with the following transformation

$$\mathbf{L} = \begin{bmatrix} \cos\phi & \sin\phi \\ -\sin\phi & \cos\phi \end{bmatrix} .$$

Next, the rays passes through the isotropic substrate on which the indicator is deposited

$$\mathbf{T}_{\text{in}} = \begin{bmatrix} t_p^{\text{in}} & 0 \\ 0 & t_s^{\text{in}} \end{bmatrix} .$$

When the rays are reflected from the magneto-optic layer, some of the s-polarization is transformed into p-polarization (and vice versa). In order to assure maximum reflection, one may evaporate a thin mirror onto the indicator. The reflection matrix from the indicator and the mirror can be expressed as

$$\mathbf{R} = \begin{bmatrix} r_{pp} & r_{ps} \\ r_{sp} & r_{ss} \end{bmatrix} ,$$

where r_{pp} and r_{ss} are the usual Fresnel coefficients. In the first order approximation (corresponding to weak magneto-optic effects), we find the following off-axis components for arbitrary magnetization vectors and angles of incidence

$$r_{ps} = \frac{\pi n_1 Q}{\lambda_0} t_{01}^s t_{10}^p \int_D f(z) \left(\frac{a(z)M_z + b(z)M_y \tan\theta_1}{M_s} \right) dz , \quad (13)$$

$$r_{sp} = -\frac{\pi n_1 Q}{\lambda_0} t_{01}^s t_{10}^p \int_D f(z) \left(\frac{a(z)M_z - b(z)M_y \tan\theta_1}{M_s} \right) dz , \quad (14)$$

where n_1 is the refractive index of indicator, Q is the magneto-optical material constant, λ_0 is the wavelength in vacuum, $t_{ij}^{s,p}$ is the s or p-component of the transmission coefficient through the interface from medium i to j (similar for $r_{ij}^{s,p}$), θ_1 is the propagation angle in the indicator, $f(z) = \exp[-i4\pi n_1 z \cos\theta_1 / \lambda_0]$, and

$$a(z) = \frac{[1 + r_{12}^s f(D - z)][1 + r_{12}^p f(D - z)]}{[1 - r_{10}^s r_{12}^s f(D)][1 - r_{10}^p r_{12}^p f(D)]} , \quad (15)$$

$$b(z) = \frac{[1 + r_{12}^s f(D - z)][1 - r_{12}^p f(D - z)]}{[1 - r_{10}^s r_{12}^s f(D)][1 - r_{10}^p r_{12}^p f(D)]} , \quad (16)$$

according to the recipe of Hubert and Traeger [21]. The integration is carried out over the thickness (D) of the indicator. Here we have neglected the transverse Kerr-effect, since this is rather small in most indicators.

For strong magneto-optical effects, one should use a similar formalism, but take into account multiple scattering. This complicates the problem considerably, and will not be pursued here.

On its way back to the array detector, the light will again pass through the substrate

$$\mathbf{T}_{\text{out}} = \begin{bmatrix} t_p^{\text{out}} & 0 \\ 0 & t_s^{\text{out}} \end{bmatrix} .$$

Furthermore, it is collected by the objective lens, and in total we can write the electric field before the analyzer as

$$E = L^{-1} T_{\text{out}} R T_{\text{in}} L E_0 . \quad (17)$$

After evaluating the equation above we observe that also the Fresnel coefficients between the substrate and air influences the polarization state of the outgoing beam. In many cases it is possible to deposit a dielectric coating which minimizes the depolarization due to the substrate. Here we assume the most ideal case, in which all transmission coefficients become unity. In this case we may write

$$E_x = \frac{1}{2}(r_{pp} + r_{ss}) + \frac{1}{2}(r_{pp} - r_{ss})\cos 2\phi - \frac{1}{2}(r_{sp} + r_{ps})\sin 2\phi , \quad (18)$$

and

$$E_y = \frac{1}{2}(r_{sp} - r_{ps}) + \frac{1}{2}(r_{pp} - r_{ss})\sin 2\phi + \frac{1}{2}(r_{sp} + r_{ps})\cos 2\phi . \quad (19)$$

These equations can be used to calculate the expected polarization pattern at the exit pupil seen in the conoscopic image, which is often used to judge the quality of the imaging system. To find the electric field at the detector plane, (r', ϕ_c) , we assume that the imaging system obeys the sine condition, and use the method of refs. [19,20] to obtain

$$E_{xD} = I_0^a + I_2^a \cos 2\phi_c + I_2^b \sin 2\phi_c , \quad (20)$$

and

$$E_{yD} = I_0^b + I_2^a \sin 2\phi_c - I_2^b \cos 2\phi_c , \quad (21)$$

where

$$I_0^a = \int_0^\alpha (r_{pp} + r_{ss}) \sin\theta \cos\theta J_0(kr' \sin\theta) \exp(2ikz \cos\theta) d\theta , \quad (22)$$

$$I_0^b = \int_0^\alpha (r_{sp} - r_{ps}) \sin\theta \cos\theta J_0(kr' \sin\theta) \exp(2ikz \cos\theta) d\theta , \quad (23)$$

$$I_2^a = \int_0^\alpha (r_{ss} - r_{pp}) \sin\theta \cos\theta J_2(kr' \sin\theta) \exp(2ikz \cos\theta) d\theta , \quad (24)$$

$$I_2^b = \int_0^\alpha (r_{sp} + r_{ps}) \sin\theta \cos\theta J_2(kr' \sin\theta) \exp(2ikz \cos\theta) d\theta . \quad (25)$$

Here J_n is the Bessel function of the first kind (of order n), and a constant in front of the integrals is omitted. Note that the integral is taken over the angular aperture of the objective lens, which has a numerical aperture $NA = \sin\alpha$. In deriving these formulas, we have assumed that the objective is corrected for all spherical aberrations introduced by the film and the substrate. Here the factor $\cos\theta$ occurs since we have chosen aplanatic apodization at the exit pupil ($\sqrt{\cos\theta}$, squared for two passes through the objective). The phase factor $\exp(i2kz \cos\theta)$ is included to account for the defocus of the light beam. Here we will assume that $z=0$, and therefore that the light beam is at focus on the mirror-plane. When an analyzer is placed in front of the detector, the intensity at the detector plane must be written as

$$i_D = |E_{xD} \cos\gamma + E_{yD} \sin\gamma|^2 , \quad (26)$$

where γ is the analyzer's angle from the x-axis. So far, we have not considered diffraction due to the localized magnetization distribution in the indicator. However, this can be included by using the procedure of Kambersky et al. [22]. In that paper a procedure for calculating the diffracted Kerr or Faraday amplitude is presented. The result must be weighted by the polarization vector of the lens system, and summed up at the exit pupil. This is a large numerical task, at least for a reflection-type microscope, and will not be pursued here. That is, we will neglect diffraction from magnetization gradients in the indicator.

IV. IMAGING OF SINGLE VORTICES IN A SUPERCONDUCTOR

Only recently magnetooptic imaging of single vortices was achieved experimentally [12]. In this section we study magnetooptic imaging of single vortices using approximative solutions of the theory given above. Interestingly, it has been found that the field from a vortex is similar to that from a magnetic monopole located a distance $z_0 = -1.27\lambda$ (λ is the penetration depth) below the superconductor surface [23]. In this approximation the scalar potential from a vortex can be written as

$$\phi_V = \frac{\Phi_0}{2\pi\mu_0} \frac{1}{\sqrt{x^2 + y^2 + (z - z_0)^2}} , \quad (27)$$

where Φ_0 is the flux quantum.

To get some insight into the behaviour of the magnetooptic response, let us neglect the absorption and the multiple reflections, and assume that $H_a \gg H_r, H_z$. Then the off-diagonal components of the reflection becomes

$$r_{ps} \propto Q t_{01}^s t_{10}^p \left\{ \frac{1}{H_a} [\phi_V(d) - \phi_V(d+D)] + D \tan \theta_1 \sin \phi_M \right\} , \quad (28)$$

and

$$r_{sp} \propto -Q t_{01}^s t_{10}^p \left\{ \frac{1}{H_a} [\phi_V(d) - \phi_V(d+D)] - D \tan \theta_1 \sin \phi_M \right\} , \quad (29)$$

where d is the distance between the superconductor and the indicator. Although these expressions are approximations, they still contain some interesting physics. Note that the second term is constant, i.e. independent of the vortex field, since we have assumed that $H_a \gg H_r, H_z$. It is also seen that the off-axis reflection coefficients are strongly dependent on the penetration depth of the superconductor. That is, when the penetration depth is large, the magnetic monopole appears to be located far from the surface of the superconductor, whereas when it is small it is located close to the surface. Thus the signal increases with decreasing penetration depth. As an example of this, Fig. 3 shows r_{ps} (without the constant term) as a function of the penetration depth when $d=125$ nm (dashed line) and $d=250$ nm (solid line). It is noted that the magnetooptical signal falls off nonlinearly with the penetration depth, but that the gradient is less severe when the distance between the superconductor and the indicator increases.

To find the actual signal at the array detector, one must evaluate Eq. 26. When the polarizer and analyzer are in nearly crossed positions ($\alpha \approx 90^\circ$), and $\phi_c = 0^\circ$, the signal can be approximated by

$$i_D \propto Q^2 \left[\phi_V^{im}(d) - \phi_V^{im}(d+D) \right]^2 \left| \int_0^\alpha t_{01}^s t_{10}^p \sin \theta \cos \theta J_0(kr' \sin \theta) d\theta \right|^2 . \quad (30)$$

Here $[\phi_V^{im}(d) - \phi_V^{im}(d+D)]^2$ may be interpreted as the geometric image of a given position (r, ϕ) at the indicator. According to the Huygens-Fresnel principle, each such point generates a spherical secondary wavelet. Since these wavelets must pass through the apertures of the optical system, the 'perfect' geometric image is smeared out at the image plane. That is, each point in the geometric image must be multiplied by a diffraction integral and the point becomes a distribution at the detector. One should also note that in the present approximation the diffraction integral is modified by the off-axis reflection coefficient through the factor $t_{01}^s t_{10}^p$. In this paper we have not considered the response of the array detector, as this is assumed to be ideal.

It is very important to note that the signal is proportional to the difference in magnetic potential at the two surfaces of the indicator. For this reason the signal increases with thickness, but the signal-distribution also broadens significantly. This issue will be of particular importance when the vortices are placed close together, and the flux-profiles overlap. Thus one may expect a thin indicator to provide better signal contrast than a thick one, in particular since the contrast is often more important than the strength of the signal. To illustrate this point, Fig. 4 shows $[\phi_V^{im}(d) - \phi_V^{im}(d+D)]^2$ at the detector plane when the vortices are placed $2 \mu m$ apart, and the thickness of the indicator is $D=5 \mu m$ (dashed line)

and $D=1\ \mu m$ (solid line). Although the signal from the thickest films is 1.7 times stronger than that of the thinnest film, we see that the contrast is better in the latter case.

Finally, it is important to point out that in deriving Eq. (30) we have done several assumptions in order to obtain a simple expression which is readily interpreted. If a detailed analysis is required, one should adopt the full formalism presented in this paper. It is our hope that this formalism could be useful for future studies on magnetooptic visualization.

V. CONCLUSION

A theoretical model for investigating magnetooptic imaging of weak magnetic fields has been presented. It takes into account the details of the indicator and the magnetooptic system. To demonstrate the applicability of the model, we have tried to understand some issues concerning imaging of single vortices in superconductors. It is found that the useful signal is strongly dependent on the penetration depth of the superconductor, and also the sensitivity and thickness of the indicator.

ACKNOWLEDGMENTS

The author is grateful to P.E. Goa, H. Hauglin, M. Baziljevich and T.H. Johansen for many interesting discussions on this topic. This work was supported by the Norwegian Research Council and Tandberg Data ASA.

REFERENCES

- [1] P.B. Alers *Phys. Rev.* **105** , 104 (1957).
- [2] H. Kirchner *Phys. Lett.* **26A** , 651 (1968).
- [3] H.U. Habermeier and H. Kronmuller *Appl. Phys.* **12** , 297 (1977).
- [4] H.U. Habermeier, W. Klein, R. Aoki and H. Kronmuller *Phys. Stat. Sol. (a)* **53** , 225 (1979).
- [5] A.V. Antonov, M.U. Gusev, E.I. Il'yashenko and L.S. Lomov *Int. Symp. on Magnetooptics (ISMO'91), USSR, Kharkov* p.70 (1991).
- [6] L.A. Jevenko, E.I. Il'yashenko, V.P. Klin, B.P. Nam and A.G. Solovyev *Int. Symp. on Magnetooptics (ISMO'91), USSR, Kharkov* p.147 (1991).
- [7] A.I. Belyaeva, A.L. Foshchan and V.P. Yur'ev *Sov. Tech. Phys. Lett.* **17**, 762 (1991).
- [8] L.A. Dorosinskii, M.V. Indenbom, V.I. Nikitenko, Y.A. Ossip'yan, A.A. Polyanskii and V.K. Vlasko-Vlasov *Physica C* **203** (1992), 149 (1992).
- [9] M.R. Koblishka and R.J. Wijngaarden , *Supercond. Sci. Technol.* **8**, 199 (1995).
- [10] A.A. Polyanskii, X.Y. Cai, D.M. Feldmann, D.C. Larbalestier, *NATO Science Series*, **3/72**, 353 (Kluwer Academic Publishers, Dordrecht 1999).
- [11] B.U. Runge, U. Bolz, J. Eisenmenger and P. Leiderer *Physica C.*, **341**, 2029 (2000).
- [12] P.E. Goa, H. Hauglin, M. Baziljevich, E.I. Il'yashenko, P.L. Gammel and T.H. Johansen *Supercond. Sci. Technol.*, **14**, 729 (2001).
- [13] L.E. Helseth, R.W. Hansen, E.I. Il'yashenko, M. Baziljevich and T.H. Johansen *Phys. Rev. B*, **64**, 174406 (2001).
- [14] V.K. Vlasko-Vlasov, Y. Lin, U. Welp, G.W. Crabtree, D.J. Miller and V.I. Nikitenko *J. Appl. Phys.*, **87**, 5828 (2000).
- [15] A.N. Egorov and S.V. Lebedev *J. Appl. Phys.*, **87**, 5362 (2000).
- [16] R.M. Grechishkin, M.Y. Gusev, S.E. Ilyashenko and N.S. Neustrov *J. Magn. Magn. Mat.* , **1996**, 305 (1996).
- [17] A. Zvezdin and V. Kotov *Modern magnetooptics and magnetooptical materials*, (IOP Publishing, Bristol, 1997)
- [18] M. Shamonin, M. Klank, O. Hagedorn and H. Dotsch *Appl. Opt.*, **40**, 3182 (2001).
- [19] L. Novotny, R.D. Grober and K. Karrai *Opt. Lett.* **26**, 789 (2001).
- [20] L.E. Helseth *Opt. Commun.* **191**, 161 (2001).
- [21] A. Hubert and G. Traeger *J. Magn. Magn. Mater.* **124**, 185 (1993).
- [22] V. Kambersky, L. Wenzel and A. Hubert *J. Magn. Magn. Mater.* **189**, 149 (1998).
- [23] G. Carneiro and E.H. Brandt *Phys. Rev. B* **61**, 6370 (2000).

FIGURES

FIG. 1. The basic setup for magnetooptical imaging.

FIG. 2. The magnetization vector in the indicator.

FIG. 3. The off-axis reflection coefficient as a function of the penetration depth when $d=125$ nm (dashed line) and $d=250$ nm (solid line). Here $D=1 \mu m$.

FIG. 4. The normalized signal from three vortices placed $2 \mu m$ apart. Here $\lambda = 100$ nm, $D=1 \mu m$ (solid line) and $D=5 \mu m$ (dashed line). We have neglected diffraction and assumed a magnification $M=1$.

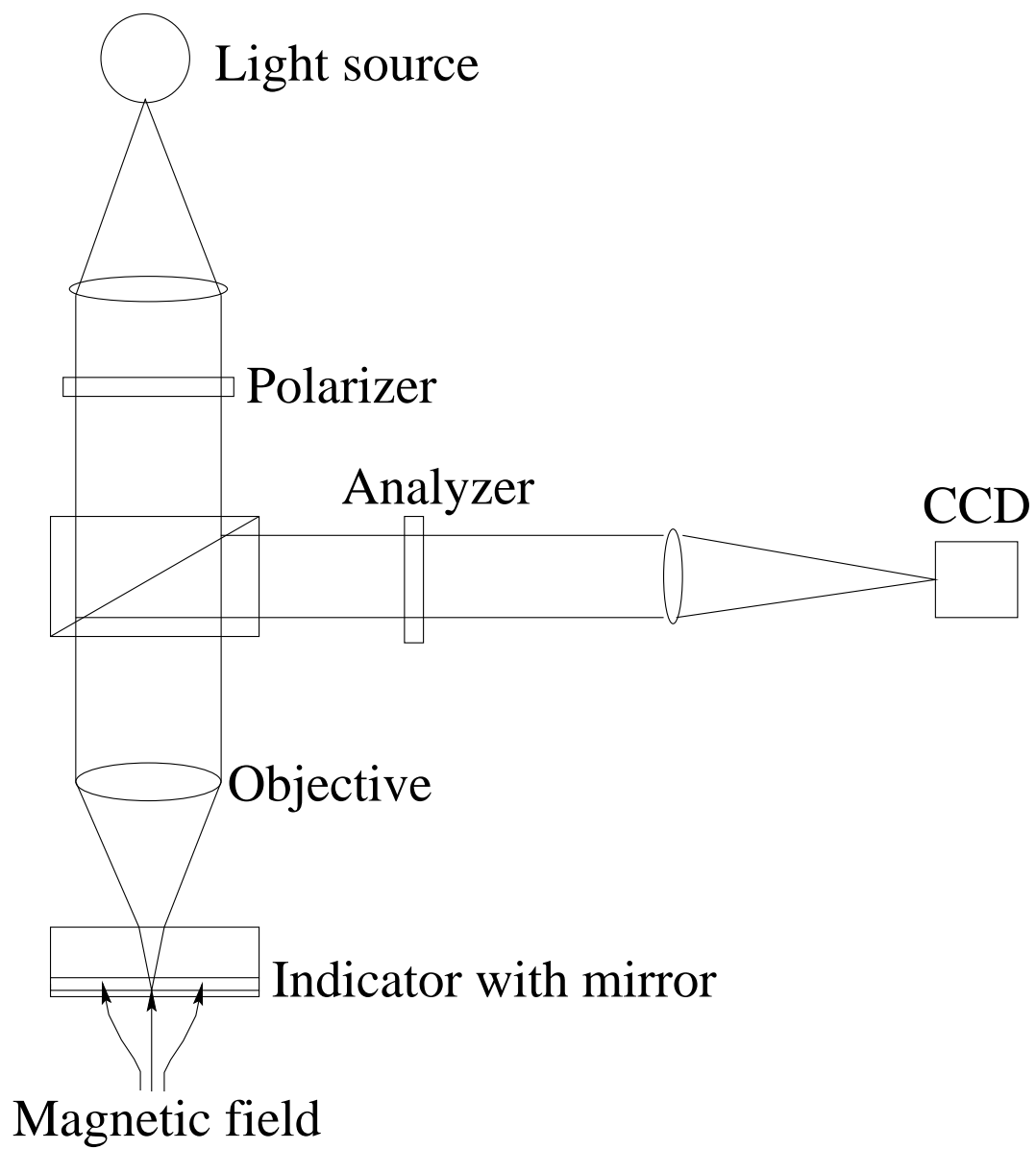


Figure 1

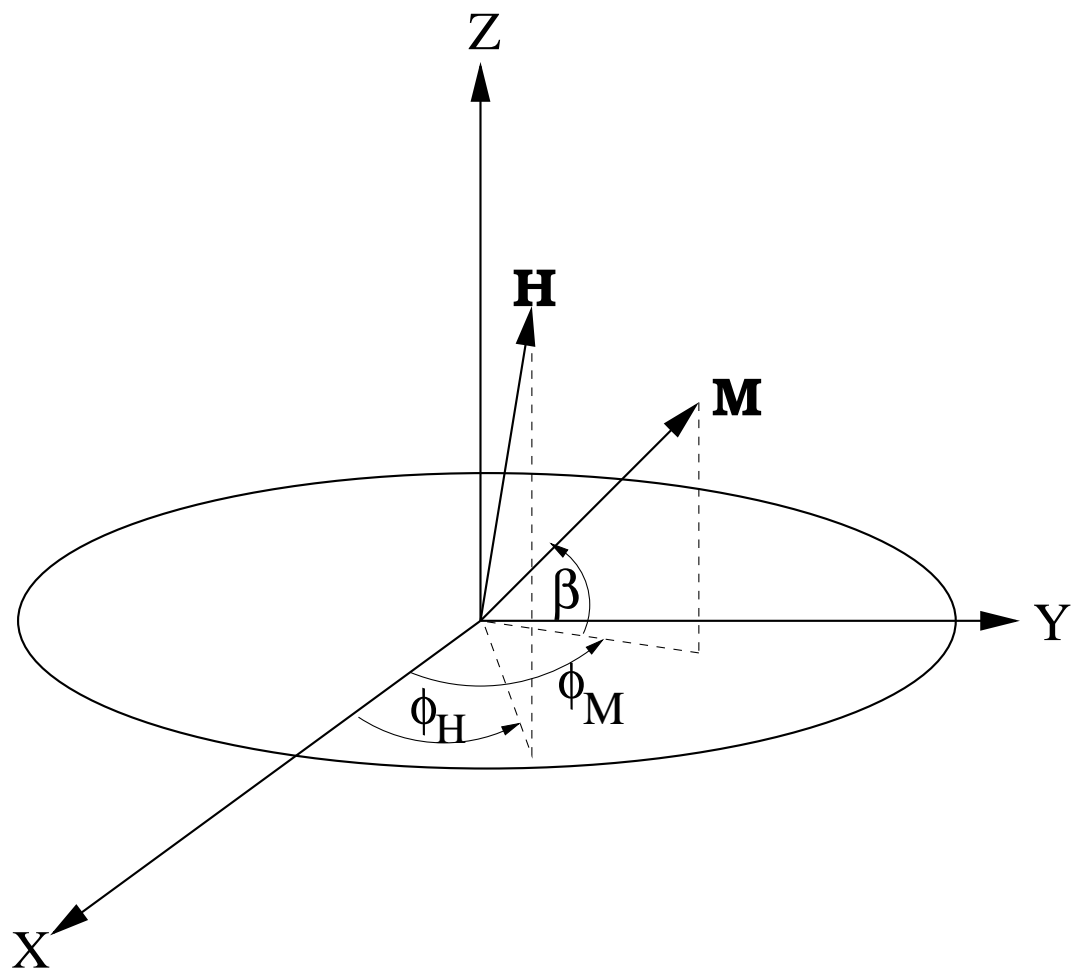


Figure 2

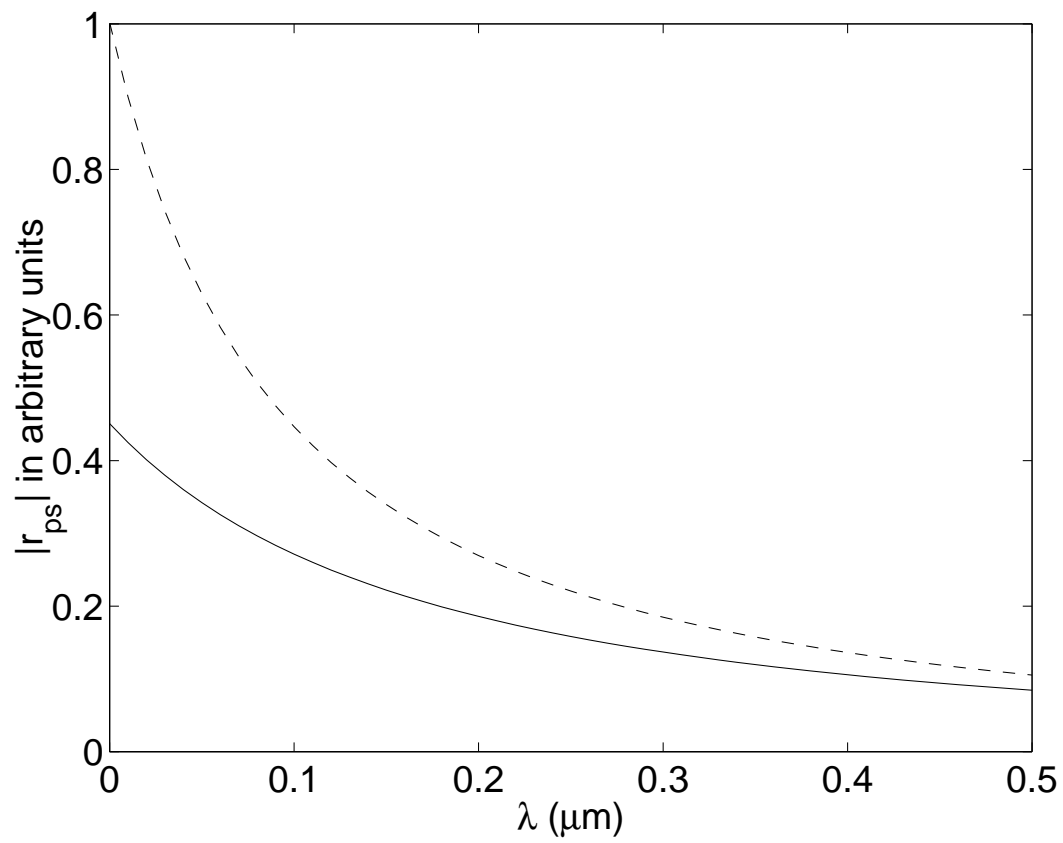


Figure 3

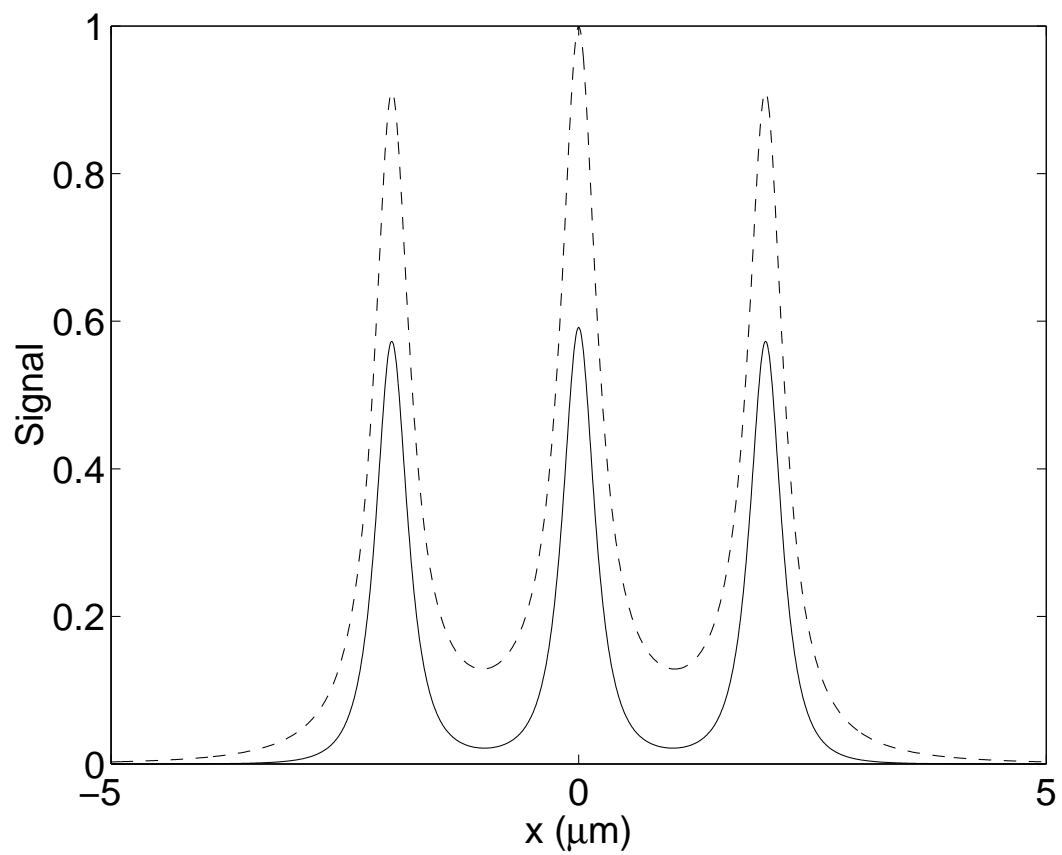


Figure 4